applied sciences

MDPI

Article

Thermal Energy Storage Performance of Tetrabutylammonium Acrylate Hydrate as Phase Change Materials

Hitoshi Kiyokawa [1], Hiroki Tokutomi [1], Shinichi Ishida [2], Hiroaki Nishi [3] and Ryo Ohmura [1,*]

[1] Department of Mechanical Engineering, Keio University, 3-14-1 Hiyoshi Kohoku-ku, Yokohama 223-8522, Japan; apalcoann@keio.jp (H.K.); konoMichini-0warihanaku@softbank.ne.jp (H.T.)
[2] Cyber Kobo LLC., 2-201, Kitabukuro-cho, Omiya-ku, Saitama-shi 330-0835, Japan; sin@cyber-lab.co.jp
[3] Department of System Design Engineering, Keio University, 3-14-1 Hiyoshi Kohoku-ku, Yokohama 223-8522, Japan; west@sd.keio.ac.jp
* Correspondence: rohmura@mech.keio.ac.jp; Tel.: +81-45-566-1813

Abstract: Kinetic characteristics of thermal energy storage (TES) using tetrabutylammonium acrylate (TBAAc) hydrate were experimentally evaluated for practical use as PCMs. Mechanical agitation or ultrasonic vibration was added to detach the hydrate adhesion on the heat exchanger, which could be a thermal resistance. The effect of the external forces also was evaluated by changing their rotation rate and frequency. When the agitation rate was 600 rpm, the system achieved TES density of 140 MJ/m^3 in 2.9 h. This value is comparable to the ideal performance of ice TES when its solid phase fraction is 45%. UA/V (U: thermal transfer coefficient, A: surface area of the heat exchange coil, V: volume of the TES medium) is known as an index of the ease of heat transfer in a heat exchanger. UA/V obtained in this study was comparable to that of other common heat exchangers, which means the equivalent performance would be available by setting the similar UA/V. In this study, we succeeded in obtaining practical data for heat storage by TBAAc hydrate. The data obtained in this study will be a great help for the practical application of hydrate heat storage in the future.

Keywords: lathrate hydrate; thermal energy storage; tetrabutylammonium acrylate (TBAAc); crystal growth; ultrasonic vibration

Citation: Kiyokawa, H.; Tokutomi, H.; Ishida, S.; Nishi, H.; Ohmura, R. Thermal Energy Storage Performance of Tetrabutylammonium Acrylate Hydrate as Phase Change Materials. *Appl. Sci.* **2021**, *11*, 4848. https://doi.org/10.3390/app11114848

Academic Editor: Ioannis Kartsonakis

Received: 17 April 2021
Accepted: 24 May 2021
Published: 25 May 2021

1. Introduction

The use of sustainable, renewable energy sources is becoming increasingly important as global attention on environmental issues increases. However, the amount of electricity generated by renewable energy sources such as wind and solar power fluctuates greatly depending on the natural environment. In recent years, energy consumption has been increasing. It is essential to have a technology to fill the gap between the amount of electricity generated and the demand. These technologies would contribute to the load leveling [1].

In particular, the recent development in information and communication technology (ICT) (e.g., Internet of Things, 5G communications, cloud computing, big data) has produced a great demand for data centers (DCs). In 2020, the rapid spread of remote working due to the pandemic also boosted demand for DCs. The industrial use of these technologies is also driving this trend [2,3]. Masanet et al. [4] estimated that the electricity use in DCs accounted for 1% of worldwide electricity use in 2020. This trend will make DCs even more energy-intensive and will increase the cost of cooling the heat generated and the amount of electricity used [5]. Considering the generalization of ICT and the widespread use of the fifth-generation mobile communication system, the amount of communication will further increase worldwide. The importance of data centers will increase to support the exchange of huge amounts of data. A suitable cooling system will be able to keep the appropriate temperature. In addition, such systems are significant to realize the zero-downtime of a DC operation with low cost.

DC cooling systems are classified into two types. One is an air-based cooling system [6,7]. The other one is a liquid cooling system [8]. As for air-based system, the heat emitted from the computer is removed by air flow. The main drawback of this system is a low thermal conductivity, less than 0.03 W m^{-1} K^{-1} [9]. On the other hand, in a liquid cooling system, the heat is removed by the thermal conduction and convection into the liquid, mostly water. A liquid cooling system is inclined to be bigger and heavier because that system utilizes only sensible heat, which has low energy density. Thermal energy storage technology is used to store the heat energy with the heat capacity of substance. When the demand of the electricity is low, the surplus electricity is stored as cold energy. Then, the stored energy is changed to electricity when the demand increases, for example, daytime peak in power usage [10,11].

Phase Change Materials (PCMs) can be a competitive system for thermal energy storage because they can also utilize latent heat, which has a higher energy density [12–16]. Organic compounds and water are representative examples of PCMs for DC cooling. As for organic PCMs, they often have problems in terms of safety. For example, paraffin is known as an organic PCM, but it is not safe because of its flammability [17]. Water is not suitable because its phase change point is outside the range of operation temperature in DCs, 288 K to 305 K [18].

Utilizing clathrate hydrate for a thermal energy storage medium has been proposed as a better idea than water or an ice-based medium [19–23]. Clathrate hydrates, ice-like compounds, are formed when some gases have contact with water or ice under high pressure and/or low temperature [24]. The gases encapsulated in clathrate hydrates are called guest compounds. Clathrate hydrates have enormous potential for industrial usage thanks to their thermodynamic properties [19,22,25–28]. Considering the application for thermal energy storage medium, equilibrium temperature should be suitable for the DC operation temperature. Favorable equilibrium temperature can be obtained appropriately by selecting the guest compounds [29–31].

Until now, only tetrabutylammonium bromide (TBAB) hydrate has been commercially applied as a hydrate PCM for air conditioning. The thermodynamic properties of TBAB hydrate have been reported in the previous studies. TBAB hydrate has an equilibrium temperature at an atmospheric pressure of 285.9 K [32], a dissociation heat of 193 kJ/kg [33], and the thermal conductivity of 0.35 W m^{-1} K^{-1} [34]. As reported by ASHRAE Technical Committee [18], the appropriate temperature range of DC cooling is 288 K to 305 K. This is why TBAB hydrate is not favorable for DC cooling.

Sakamoto et al. [35] studied the thermodynamic properties of tetrabutylammonium acrylate (TBAAc) hydrate. According to the study, TBAAc hydrate had the highest equilibrium temperature of 291.5 K at w_{TBAAc} = 0.36, where w_{TBAAc} is the mass fraction of TBAAc. The greatest dissociation heat, a latent heat, of 195 kJ/kg was obtained at w_{TBAAc} = 0.33 under ambient pressure. As for the thermal conductivity of ionic semiclathrate hydrates, Fujiura et al. [34] studied the value of tetrabutylammonium bromide (TBAB) hydrate and tetrabutylammonium chloride (TBAC) hydrate, which have similar characteristics with TBAAc hydrate. They reported that TBAB hydrate and TBAC hydrate have thermal conductivity of approximately 0.40 W m^{-1} K^{-1}. According to the report by ASHRAE Technical Committee [18], the cooling system for DCs is required to be set from 288 K to 305 K. From the aspect of operation temperature in DCs, it can be said that TBAAc hydrates are suitable for utilizing in DC cooling as PCMs. Also, the dissociation heat of the TBAAc is larger than that of TBAB hydrate, which has been commercialized in the industrial area [33,35]. Given these advantages, TBAAc hydrates could be better PCMs for DC cooling. This is why it has significant meaning to practically evaluate the performance of TBAAc hydrates as PCMs. As a step for industrial use of TBAAc hydrate, we performed kinetic thermal energy storage experiments with TBAAc hydrate.

Based on these results, we obtained the data of energy storage density and energy storage rate during the experiments. During the experiments, we also found the adhesion of the hydrate to the surface of the heat exchanger. As the adhered hydrate is the thermal

resistance to the further hydrate formation, we used an agitator or an ultrasonic transducer to break the adhesion. By comparing the data with and without external forces, such as the agitation and ultrasonic waves, we obtained the practical data for a hydrate-based thermal energy storage system in DC cooling.

2. Materials and Methods

2.1. Materials

The details on reagents used in this study were summarized in Table 1. Tetrabutylammonium Acrylate (TBAAc) aqueous solution was obtained by neutralizing Tetrabuthylammonium hydroxide (TBAOH) aqueous solution, 1.52 kg, (0.40 mass fraction, Sigma Aldrich Xo. LLC, Saint Louis, MO, USA) and Acrylic acid, 0.17 kg, (0.99 mass fraction in liquid reagent, Sigma Aldrich Xo. LLC, Saint Louis, State of MO, USA). Also, we added laboratory-made H_2O, 0.35 kg. The mass fraction of TBAAc (w_{TBAA_c})) was 0.36. The masses of all reagents were measured by an electronic balance (GF-600, A&D Co. Ltd., Tokyo, Japan) with an expanded uncertainty of ± 0.004 g (coverage factor, k = 2).

Table 1. Specification of the reagents used in this study.

Name	Chemical Formula	Supplier	Purity
Tetrabuthylammonium hydroxide	$(CH_3CH_2CH_2CH_2)_4NOH$	Sigma-Aldrich Co. LLC	0.40 mass fraction in aqueous solution
Acrylic acid	CH_2=CHCOOH	Sigma-Aldrich Co. LLC	0.99 mass fraction in liquid reagent
Tetrabuthylammonium Acrylate	$(CH_3CH_2CH_2CH_2)_4NOOCHC=CH_2$	Laboratory made from above solution	0.36 mass fraction in aqueous solution after the neutralization process The standard uncertainty of mass fraction was ± 1.0×10^{-4}
Water	H_2O	Laboratory made	Electrical conductivity was less than 0.1 μS/cm

2.2. Apparatus

The schematic diagram of the experimental apparatus is illustrated in Figure 1. The insulating container's width, length and height are all 150 mm. Cooling water was circulated inside a copper coil tube (inner diameter 6.35 mm, outer diameter 4.35 mm) for heat exchange. This coil's diameter, pitch and number of turns are 100 mm, 10 mm, and 7 times, respectively. The temperature and flow rate in the coil was controlled by a chiller (CTP-3000 EYELA, Tokyo Rikakikai Co. Ltd., Tokyo, Japan) and flowmeter with a precision needle valve (RK 1250, KOFLOC Kyoto, Kyoto, Japan). As shown in Figure 1, the temperature of cooling water and TBAAc were measured by three platinum resistance temperature detectors (222-055, Electronic Temperature Instrument Ltd., West Sussex, UK) with an uncertainty of ± 0.1 K (k = 2). The surface of the coil would be covered with hydrate during the experiment. This hydrate prevents the heat exchange between the heat exchanger and thermal energy storage medium. We used an ultrasonic transducer (HEC-45282, HONDA Electronics Co. Ltd., Tokyo, Japan) or an agitator (SM-103D, Kenis Ltd., Osaka, Japan) to prevent the hydrate deposition.

2.3. Procedures

We made 2.0 kg of TBAAc aqueous solution by mixing the above reagents and put them in the container. The entire system was confirmed to be stationary at 298 K. T_{in} (outlet of the chiller) and flow rate, $\dot{V}_w$, of the cooling water were controlled at 291 K and 5.0×10^{-4} m^3/min. Then, we started the thermal energy storage with TBAAc hydrate. We set t = 0 when we started the circulation of the cooling water. The time evolution of T_{in},

T_{out} (temperature at inlet of the chiller) and T_{PCM} were measured every 10 s to evaluate the kinetic aspect of TBAAc hydrate as a thermal energy storage medium.

We performed such experiments in three systems. First, we did not add any external forces to the apparatus. Second, we used a rotating-impeller agitator to break adhesions between the hydrate and the coil. Third, we used the ultrasonic wave instead of mechanical agitation. In the system where the agitator was used, we also investigated the effect of rotation rate of the agitator by changing the rate to 100 rpm, 300 rpm and 600 rpm. Similarly, we investigated the effect of the frequency of ultrasonic waves on the system by changing the frequency. The frequency was set at either 28 kHz or 56 kHz.

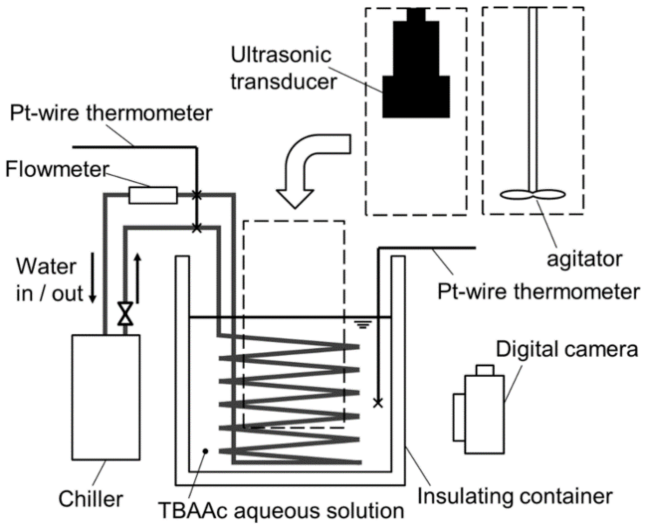

Figure 1. Schematic diagram of the apparatus.

3. Results and Discussion

3.1. The System without Any External Forces (Static System)

Initially, we reported the thermographs of Tetrabutylammonium Acrylate (TBAAc) hydrate obtained by a differential scanning calorimeter (DSC). Figure 2 shows the thermographs, which were measured at w_{TBAAc} = 0.33 and 0.36. A single peak was observed, and the existence of ice was not identified at w_{TBAAc} = 0.33.

As for the system without any external forces (static system), we performed thermal energy storage experiments. We measured T_{in}, T_{out}, and T_{PCM}. Figure 3 shows the time evolution of each temperature. Time zero indicates the time at which the circulating water is started to flow inside the coil. As shown in Figure 3, T_{PCM} decreased until t = 1.5 h and increased from t = 1.5 to t = 4 h. When T_{PCM} is increasing, TBAAc hydrate formation would occur because the T_{PCM} was 10 K lower than its equilibrium temperature, 291.5 K [35]. After the hydrate formation, the heat generation from the hydrate formation occurred and exceeded the endothermic of the heat exchanger. This was why T_{PCM} rose from t = 1.5 to t = 4 h. T_{PCM} moderately decreased again at t = 4 h when T_{PCM} was 288 K. At this moment, the formed TBAAc hydrate gradually grew around the heat exchanger as shown in Figure 4d. This adhesion would be the thermal resistance between the heat exchanger and thermal energy storage medium much lower than before. Then, the hydrate formation rate decreased due to the increased thermal resistance, and T_{PCM} decreased because the endothermic of the heat exchanger exceeds the heat generation from hydrate formation.

Figure 4a–d illustrates the optical observation of the time evolution of the hydrate formation. The hydrate was formed on the surface of the heat exchanger. Heat exchange occurs on the heat exchanger surface, which leads to hydrate formation occurring there. From t = 1.5 h to t = 2 h, the hydrate gradually grew and started covering the coil surface. The surface of the coil was fully covered by the hydrate around t = 4 h. After t = 7 h, optical changes could not be observed. In addition, we found that the TBAAc hydrate

kept growing from the surface of the coil to the bulk of the solution. There was a 3 cm gap between the surface of the coil and the wall of the container. This discovery of the hydrate growth length can be a tip to design a static thermal energy storage system. Thermal energy storage rate, $\dot{q}$, and density, $\bar{q}$, were calculated by the formulas (1) and (2). What every character stands for is written in Table 2. On the right-hand side of (2), the thermal energy storage density due to sensible heat is subtracted from the thermal energy storage density, which is obtained by integrating the thermal energy storage rate.

$$\dot{q} = \rho_w \dot{V}_w c_w (T_{out} - T_{in}) / V_{PCM} \quad (1)$$

$$\bar{q} = \sum_{t=0}^{t} \dot{q} dt - \rho_{PCM} c_{PCM} (T_{PCM,\,0} - T_{PCM}) \quad (2)$$

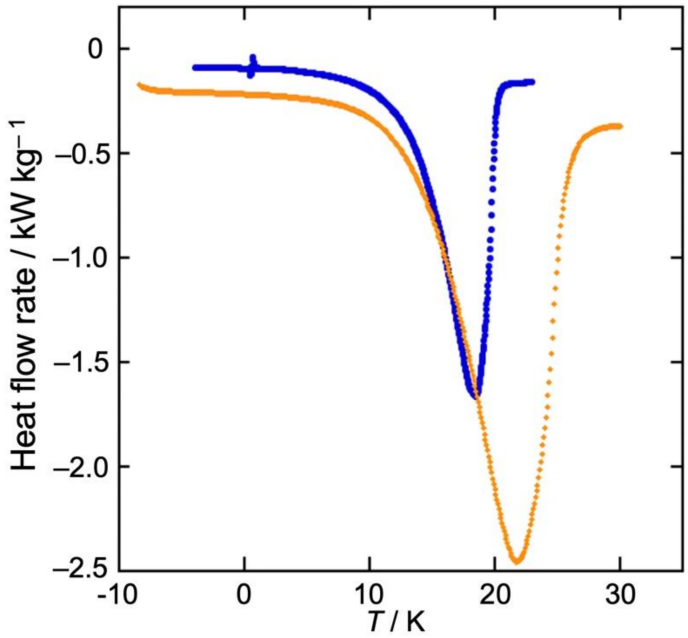

Figure 2. The DSC heating curves measured at w_{TBAAc} = 0.33 and 0.36. ●: w_{TBAAc} = 0.36, ◆: w_{TBAAc} = 0.33.

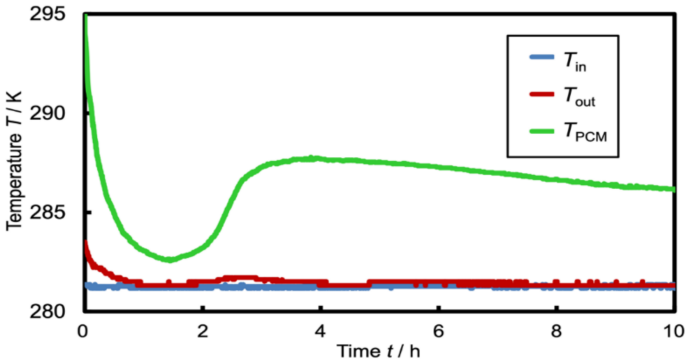

Figure 3. Time evolutions of the temperature at inlet of the chiller (T_{in}), outlet (T_{out}) of the chiller and thermal energy storage medium (T_{PCM}) in the static system.

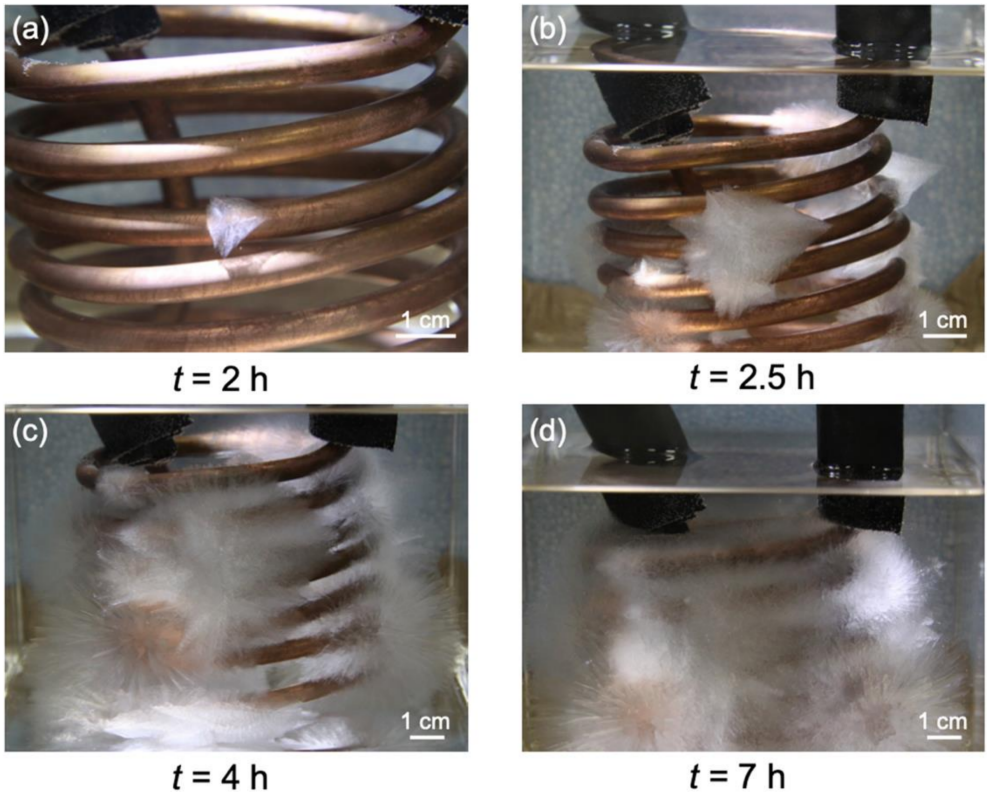

Figure 4. Crystal growth of TBAAc hydrate on the surface of the heat exchanger coil. (**a**–**d**) illustrate the optical measurement of the hydrate formation at t = 2, t = 2.5, t = 4 and t = 7, respectively.

Table 2. The value of each parameter in the calculation.

Parameter	
Density, ρ_w (Water)	999.8 kg/m^3
Volumetric flow rate, $\dot{V_w}$ (Water)	8.3×10^{-5} m^3/s
Specific heat at constant pressure, c_w (Water)	4.20 kJ/(kg K)
Density, ρ_{PCM} (PCM)	1.0 kg/m^3
Specific heat at constant pressure, c_{PCM} (PCM)	4.20 kJ/(kg K)

The obtained thermal energy storage density represents the heat storage density due to heat of hydrate formation and decomposition. The density of the PCM is assumed to be 1.0 kg m^{-3}. The value of each parameter used in the calculation is shown in Table 2. The physical property of water was referred to REFPROP ver. 9.1 [36].

Figure 5a illustrates the time evolution of the thermal energy storage rate in the static system. Since $\dot{q}$ is proportional to the gap between T_{in} and T_{out}, $\dot{q}$ varied the same way with T_{out}. Immediately after the start of the experiment, $\dot{q}$ decreased as T_{out} decreased, and as T_{out} approached T_{in}, $\dot{q}$ approached 0. After that, $\dot{q}$ increased at t = 1.5 h and reached around 9 kW/m^3. This is due to the increase in T_{out} caused by the heat generation from hydrate formation and growth, as described above. After t = 3 h, as T_{out} descended to be tangent to T_{in}, $\dot{q}$ descended to 0 with some fluctuations. Figure 5b illustrates the time evolution of thermal energy storage density. Since $\overline{q}$ indicates the thermal energy density by hydrate growth and decomposition, there is no change right after the experiments start. As the hydrate grew, thermal energy storage density increased. The rate of increase gradually became slower. The hydrate formation rate got slower due to the decreased heat

conductivity around the heat exchanger coil. This is why the increasing rate of thermal energy storage density decreased. Thermal energy density reached 96 MJ/m^3 in 10 h.

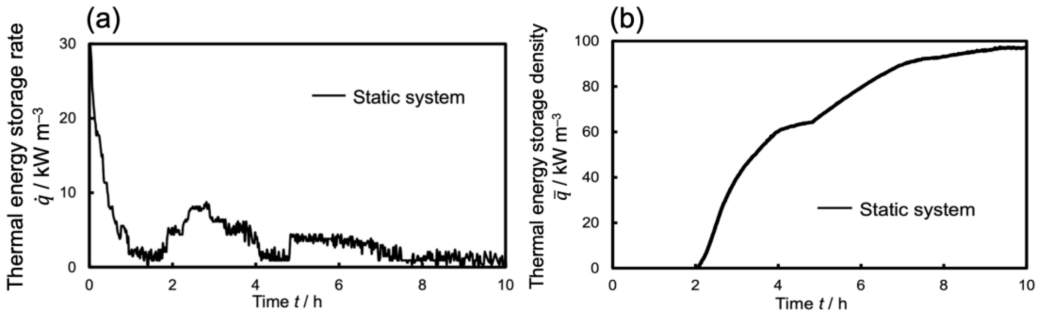

Figure 5. Time evolution of thermal energy storage rate and density in static system. (**a**,**b**) depict the thermal energy storage rate and density, respectively.

It is known that the solid phase fraction of ice thermal storage increases significantly with time up to around 30%, but the increasing rate decreases after about 40–50%. Therefore, it is favorable to design a thermal energy storage system that has a solid phase fraction of 40–50% [37]. For example, when the solid phase fraction is 45% in an ice thermal energy storage system, thermal energy storage density is approximately 140 MJ/m^3. Oyama et al. [33] reported that TBAB hydrate, which is the only commercially available hydrate PCM, has the heat for formation and decomposition of approximately 200 MJ/m^3. Assuming the TBAAc hydrate has 200 MJ/m^3 of heat in hydrate formation and decomposition, the thermal energy storage density corresponds to a solid phase fraction of 48%.

3.2. In the System with Mechanical Agitation

As written in 3.1., the surface of the heat exchanger coil was covered by hydrate. This hydrate adhesion increased thermal resistance. To solve this problem, mechanical agitation was used. In addition, to investigate the effect of the rotation rate, we changed the rate to 100 rpm, 300 rpm and 600 rpm. Figure 6a–c shows the time evolution of T_{in}, T_{out} and T_{PCM} in each rotation rate. Time zero was defined as the time at which the circulating water is started to be flown. In every rotation rate, T_{PCM} decreased twice after the experiment started and temporarily increased. In the agitated system, T_{PCM} increased earlier than the static system. As the rotation rate became quicker, T_{PCM} increased earlier. When T_{PCM} increased, the temperature was around 282 K, which is the same as the static system. This result indicates that the forced convection generated by the agitation increased the convective heat transfer coefficient, which resulted in faster cooling of the heat storage medium and thus faster nucleation. T_{PCM} increased rapidly more than the static system, which was almost vertically to around 288 K. This would be due to the increase in heat and mass transfer rates caused by the forced convection generated by the agitation, which led to the increase in the hydrate growth rate.

T_{PCM} changed from a rise to a fall around 288 K and then descended slowly. As the hydrate grew, the viscosity of the heat storage medium increased and the forced convection was weakened, which lowered the hydrate formation rate. T_{PCM} decreased because the hydrate growth rate became smaller, and the heat absorption by the heat exchanger exceeded the heat generated from hydrate formation.

Figure 7a–c shows the pictures of crystal growth in the system when the mechanical agitation rate was 300 rpm. At t = 0.6 h, numerous small crystals began to float in the aqueous solution. After t = 0.7 h, hydrate was formed in the entire aqueous solution. The hydrate nucleation occurred in the entire aqueous solution. This was because of the forced convection generated by the agitation, which stripped the hydrate from the heat exchange coil and suspended it in the aqueous solution. This convection increased the hydrate growth rate as well. Within a few minutes, the heat exchange coil was only faintly visible

by the hydrate, as shown in Figure 7b. The hydrate formation has progressed and the viscosity increased as shown in Figure 7c, after which little change was observed.

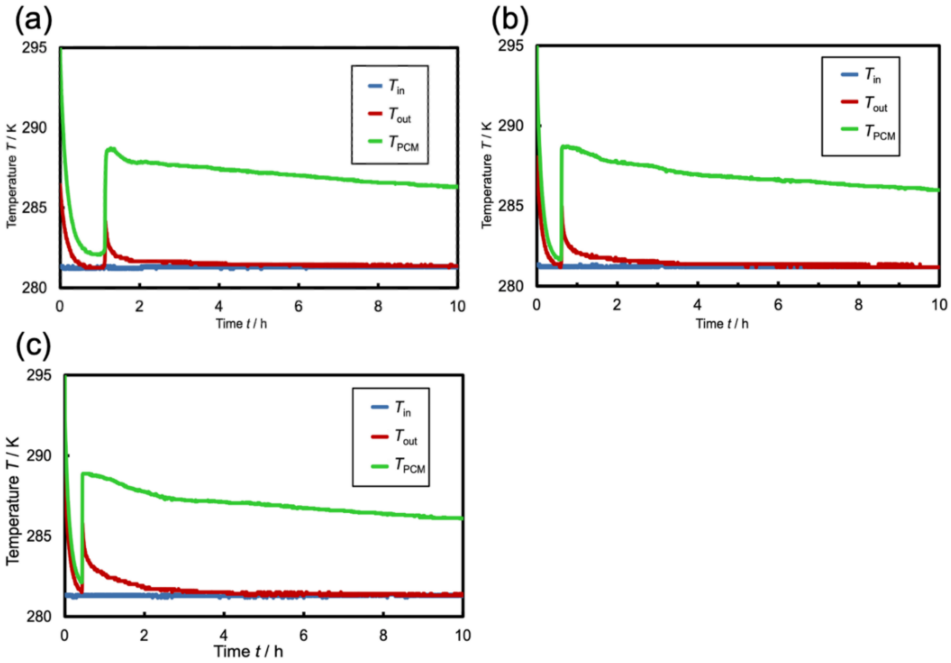

Figure 6. Time evolutions of the temperature at inlet of the chiller (T_{in}), outlet (T_{out}) of the chiller and thermal energy storage medium (T_{PCM}) in the system with the mechanical agitation. (**a**–**c**) depict each curve at the agitation rate of 100 rpm, 300 rpm and 600 rpm, respectively.

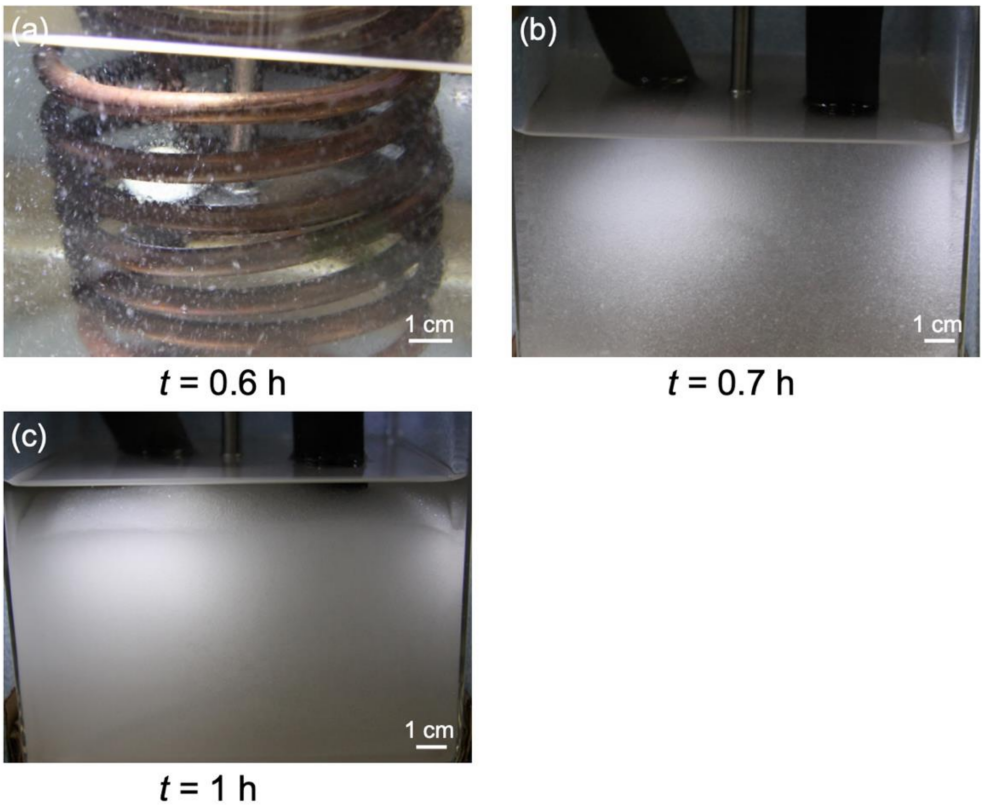

Figure 7. Optical observation changing in the container with mechanical agitation of 300 rpm. (**a**–**c**) are the pictures at 0.6 h, 0.7 h and 1 h after cooling water started to be circulated, re-spectively.

We visually observed that TBAAc hydrate formed and grew to the bulk of the solution. The gap between the heat transfer surface and the corner of the container was about 5 cm. In other words, when the cooling temperature was 10 K lower than the equilibrium temperature, TBAAc hydrate formed and grew at a distance of more than 5 cm from the heat transfer surface in the agitated system. The same tendency was observed at the rotation rate of 100 rpm and 600 rpm.

Figure 8a shows the time evolution of thermal energy storage density. To make a comparison with the static system, the time evolution of the static system is also shown in Figure 8a. Regarding the thermal energy storage rate, $\dot{q}$ is proportional to the difference between the inflow temperature T_{in} and the outflow temperature T_{out}. This was why $\dot{q}$ had almost the same trend as the T_{out} change in the static system. As T_{out} increased rapidly more than the static system, $\dot{q}$ increased rapidly more than the static system as well, rising almost vertically. The maximum thermal energy storage rate at that time was about 6 to 8 times faster than that of the static system. The larger the rotation rate of the agitation increased the value of $\dot{q}$. After a rapid increase, the change in $\dot{q}$ suddenly turned into a downward movement and gradually descended to 0. This was because the hydrate had grown, and the viscosity had increased, which resulted in less convection.

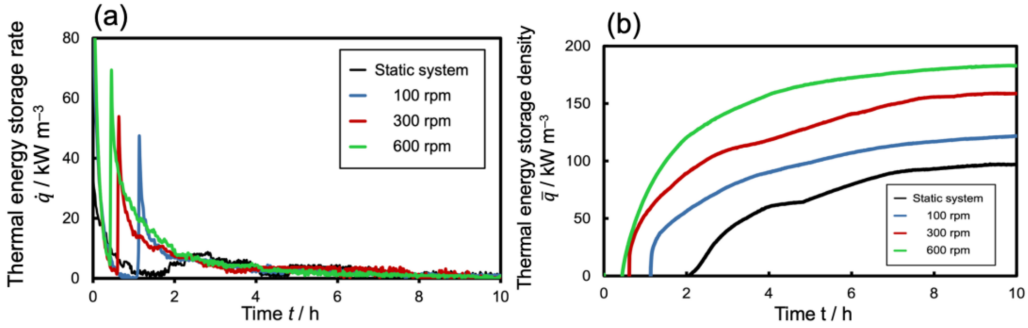

Figure 8. Time evolution of thermal energy storage rate and density in the agitated system (**a**,**b**) depict the thermal energy storage rate and density, respectively.

As shown in Figure 8b, $\bar{q}$ in the agitated system increased earlier than that in the static system, and the higher rotation rate of the agitation increased $\bar{q}$ earlier. This was because the temperature of the thermal energy storage medium was lowered quickly by forced convection, and thus hydrate nucleation also occurred quickly. The thermal energy storage density $\bar{q}$ was larger than that of the static system and increased by a higher rotation rate. This was because the forced convection caused by the agitation allowed hydrate to be formed in the entire bulk of the solution. In the agitated system with the rotation rates of 100 rpm, 300 rpm and 600 rpm, thermal energy density reached 121 MJ/m^3, 159 MJ/m^3 and 183 MJ/m^3 in 10 h, respectively. Similarly, assuming the TBAAc hydrate has 200 MJ/m^3 of heat in hydrate formation and decomposition, the thermal energy storage density corresponds to a solid phase fraction of 61%, 80% and 92%, respectively.

3.3. In the System Using an Ultrasonic Transducer

In this section, we discuss the results in the system with ultrasonic vibration. The inflow temperature T_{in}, outflow temperature T_{out} and thermal energy storage medium temperature T_{PCM} were measured. Figure 9a,b shows the time evolutions of T_{in}, T_{out} and T_{PCM} in the ultrasonic vibration system (28 kHz and 56 kHz). Time zero was defined as the time at which the circulating water was started to flow.

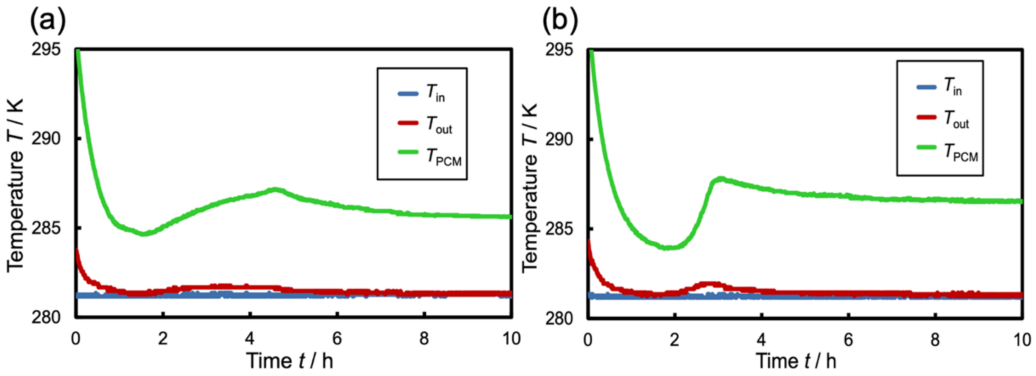

Figure 9. Time evolutions of the temperature at inlet of the chiller (T_{in}), outlet (T_{out}) of the chiller and thermal energy storage medium (T_{PCM}) in the system with ultrasonic vibration. (**a**,**b**) depict each curve at the frequency of 28 kHz and 56 kHz, respectively.

The slope of the T_{PCM} first decrease was similar to that of the static system. However, when the slope changed from negative to positive, the T_{PCM} was about 284 K, which was higher than that of the static and agitated system. This is because the hydrate nucleation occurred at a higher temperature than in the static system. In an ultrasonic vibration system, hydrate nucleation would occur at a higher temperature due to the effects of cavitation or acceleration of ultrasonic vibration.

The slope of the T_{PCM} increase is not much different from that of the static system at 28 kHz and appears to be more gradual at 56 kHz. This was because of relatively high T_{PCM}, which results in a relatively slow hydrate growth rate and low heat of formation during hydrate nucleation. The increase in T_{PCM} changed from a rise to a fall at around 288 K, and then T_{PCM} slowly decreased. This was because the slope of the T_{PCM} change turned from positive to negative because hydrate was generated and covered the heat exchange coil surface as the static system.

Figure 10a–c shows the pictures of the crystal growth during this system. As shown in Figure 10a–c, hydrate was formed on the heat transfer surface near the bottom of the container. As time went by, the formed hydrate piled up on the bottom of the container. Figure 11a shows time evolutions of thermal energy storage rate in the system using the ultrasonic vibration, which depends on the frequency of 28 kHz and 56 kHz. The thermal energy storage rate $\dot{q}$ in the static system is also shown for comparison. Time zero was defined as the time at which the circulating water is started to flow. Here, $\dot{q}$ was proportional to the difference between T_{in} and T_{out} and thus shows almost the same trend as T_{out} change in the static system. In addition, the slope of change in the thermal energy storage rate was similar to that of the static system. However, as for the 28 kHz ultrasonic vibration, the maximum value of $\dot{q}$ after the increase was about 1.5 times larger than that of the static system. This was because the hydrate was detached from the heat exchange coil by cavitation, which increased the growth rate of the hydrate. On the other hand, the maximum value of $\dot{q}$ at 56 kHz was almost the same as that of the stationary system. Considering the size of hydrate adhesion, the cavitation effect is stronger at lower frequencies. This was why the maximum value of $\dot{q}$ at 56 kHz was larger than that of $\dot{q}$ at 28 kHz. After the peak of $\dot{q}$, the ultrasonic vibration system maintained a larger $\dot{q}$ for a relatively longer time than the static system. This was because the hydrate growth was continued for a relatively long time after the hydrate covered the heat exchange coil due to the effects of cavitation. Figure 11b shows the time evolution of the thermal energy storage density. The result of the static system is also shown in Figure 11b. Time zero was defined as the time at which the circulating water is started to flow. As shown in Figure 11b, $\overline{q}$ in the ultrasonic vibrated system started increasing a bit earlier than the static system. This was because the cavitation enabled the hydrate to be formed at a higher temperature. The slope of $\overline{q}$ change in the ultrasonic vibration system is almost the same as with the static system. However, the bigger slope could be kept longer than the static system. This was also

because the hydrate growth could be kept by the effect of the cavitation. In the ultrasonic vibration system with a frequency of 28 kHz and 56 kHz, thermal energy storage density reached 126 MJ/m^3, 111 MJ/m^3 in 10 h, respectively. Similarly, assuming the TBAAc hydrate has 200 MJ/m^3 of heat in hydrate formation and decomposition, the thermal energy storage density corresponds to a solid phase fraction of 63% and 55%, respectively.

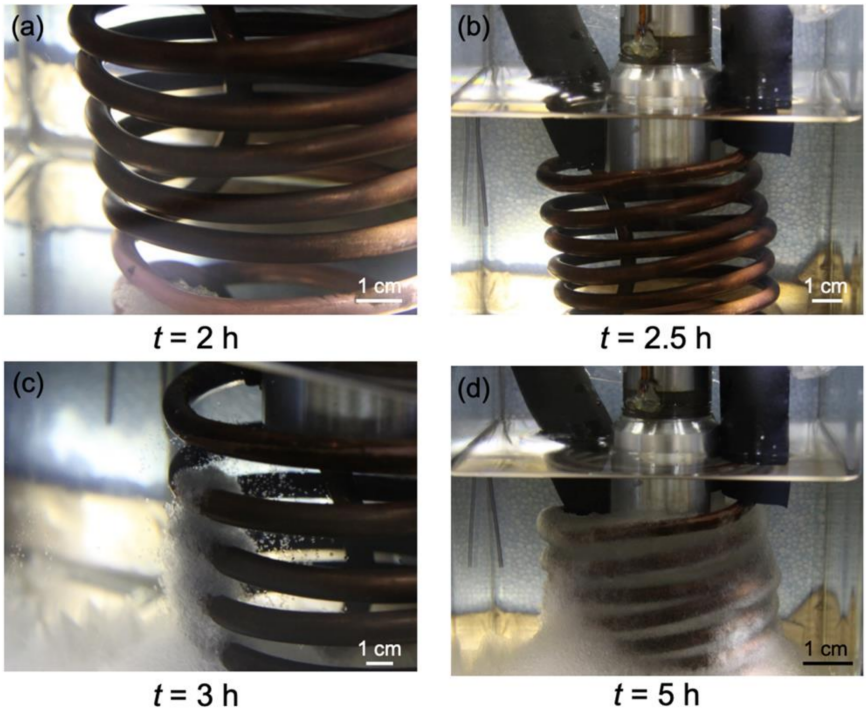

Figure 10. Optical observation changing in the container with ultrasonic vibration of 28 kHz. (**a**–**d**) are the pictures at 2 h, 2.5 h, 3 h and 5 h after cooling water started to be circulated, respectively.

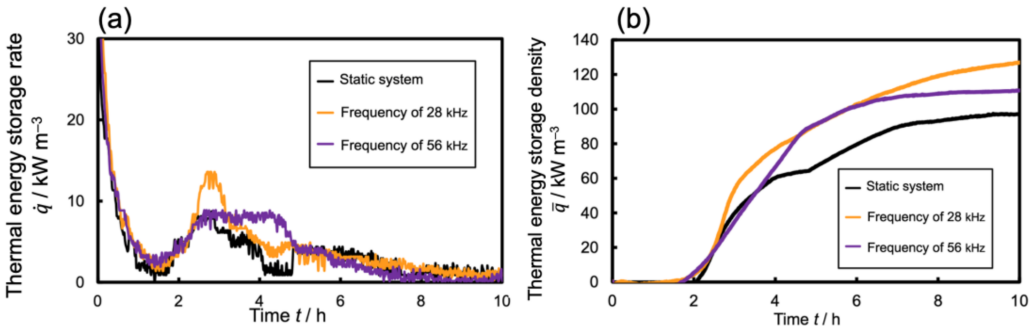

Figure 11. Time evolutions of the thermal energy storage rate and density in the system using an ultrasonic vibration. (**a**,**b**) depict the thermal energy storage rate and density, respectively.

3.4. Comparison in All Systems

Figure 12a shows a comparison in the time evolution of the thermal energy storage rate in all systems. In the agitated system, the thermal energy storage rate, $\dot{q}$, increased earlier than the other systems; $\dot{q}$ increased at 1 h, 0.6 and 0.4 h for a rotation rate of 100 rpm, 300 rpm and 600 rpm, respectively. The forced convection generated by the agitation increased the convective heat transfer coefficient. This was why the temperature of the thermal energy storage medium dropped relatively earlier and hydrate formation occurred earlier, resulting in the early increase of $\dot{q}$. In addition, this forced convection caused rapid hydrate formation in the entire container, which released huge heat in a short period. This was why $\dot{q}$ increased vertically. As the rotation rate increased, $\dot{q}$ increased more.

The maximum values of $\dot{q}$ after the vertical increase were 47 kW m^{-3}, 54 kW m^{-3} and 69 kW m^{-3} for a rotation rate of 100 rpm, 300 rpm and 600 rpm, respectively. These values are 5 to 8 times larger than that of a static system.

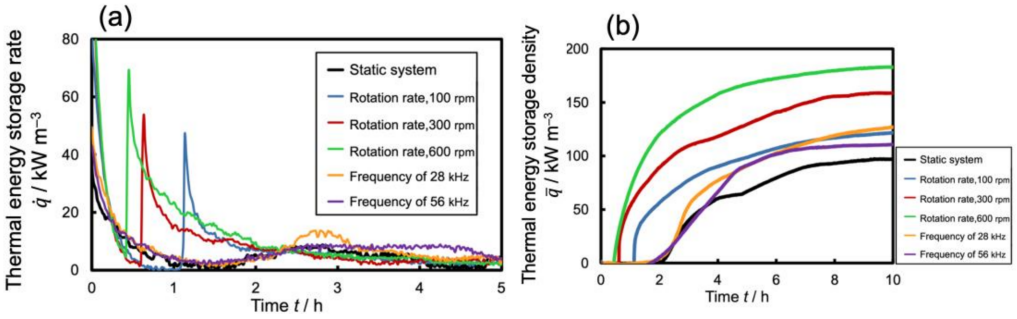

Figure 12. Time evolutions of thermal energy storage rate and density in all systems. (**a**,**b**) depict the thermal energy storage rate and density, respectively.

In the ultrasonic vibration system, the maximum of $\dot{q}$ was 14 kW m^{-3}, which is about 1.5 times larger than that of the static system, when the frequency was 28 kHz. This was because cavitation detached the adhesion between hydrate and heat exchanger coil, which could be the thermal resistance. As for the system with 56 kHz frequency, the maximum values of $\dot{q}$ were almost the same as in the static system. This was because the effect of the cavitation was not as big as 28 kHz [38]. In summary, the agitation increased the rate of heat and mass transfer by creating forced convection, thereby shortening the hydrate formation time and increasing the hydrate growth rate. On the other hand, ultrasonic vibration kept the hydrate growth longer by the effect of cavitation.

Figure 12b shows a comparison in the time evolution of thermal energy storage density, $\bar{q}$, in all systems. In the agitated system, $\bar{q}$ increased earlier and quicker than the other systems. This was because T_{PCM} decreased quicker by the forced convection, which caused the quicker hydrate formation and growth for the entire container. In the ultrasonic vibration system, the $\bar{q}$ increase appeared to be relatively longer than the other systems. This was because the cavitation enabled hydrate to grow after hydrate covered the surface of the heat exchanger coil. The static system, the agitated system (rotation rate of 100 rpm, 300 rpm and 600 rpm), and the ultrasonic vibrated system (frequency of 28 kHz and 56 kHz) had the thermal energy storage density of 96 MJ/m^3, 121 MJ/m^3, 159 MJ/m^3, 183 MJ/m^3, 126 MJ/m^3, and 111 MJ/m^3, respectively. Assuming TBAAc hydrate has the heat for formation and decomposition of approximately 200 MJ/m^3, each solid phase fraction is 48%, 61%, 80%, 92%, 63%, and 55%, respectively.

3.5. For Industrial Utilizing of TBAAc Hydrate as PCM

As written in Section 3.1., a range of the practical solid-phase fraction is from 40 to 50% [37]. The thermal energy storage density of ice is 140 MJ m^{-3} when the solid phase fraction is 45%. As for TBAB hydrate, it has a thermal energy storage density of 100 MJ/m^3 when the solid phase fraction is 50% [33]. We regarded these values as a target thermal energy storage density. Given the thermal energy storage during nighttime of 10 h, the required time for thermal energy storage should be shortened. This was why the time to reach the target values was compared to each other system. In addition, the amount of the used electric power was estimated for more practical evaluation.

Table 3 shows the time that was needed to achieve the target thermal energy storage density. As for the target of 140 MJ/m^3, it was achieved only when the rotation rates of agitation were 300 rpm and 600 rpm. When the rotation rates were 300 rpm or 600 rpm, it was 5.9 h or 2.9 h to achieve the target, respectively. Concerning the consumed electric power to achieve the target, it was 58 MJ/m^3 and 29 MJ/m^3, respectively. As for the target of 100 MJ/m^3, it was achieved in all systems where an external force was applied. When the rotation rates were 300 rpm and 600 rpm, it took about a third of the time of

the ultrasonic vibration system. However, the consumed electric power by the external force to achieve the target was 45 MJ/m^3, 24 MJ/m^3, 15 MJ/m^3 for the agitation system (100 rpm, 300 rpm, 600 rpm), and 5 MJ/m^3 for the ultrasonic vibration system at both frequencies (28 kHz, 56 kHz), respectively. Therefore, when the target of thermal energy storage density is 100 MJ/m^3, the agitation system (300 rpm, 600 rpm) is more suitable for storing thermal energy in a short time, and the ultrasonic vibration system is more suitable as an external force for reducing the amount of electricity used.

Table 3. The time to achieve the target thermal energy storage density.

Target	Static System	Agitated System			Ultrasonic Vibrated System	
		100 rpm	300 rpm	600 rpm	28 kHz	56 kHz
100 MJ/m^3 Achieved time/h	-	5.1	2.4	1.5	5.8	5.8
140 MJ/m^3 Achieved time/h	-	-	5.9	2.9	-	-

In this study, the thermal energy storage density in the agitated system was greatly improved by adding agitation. On the other hand, the amount of electricity used for agitation became larger than other systems. The agitation intensity was almost the same as that in a general low-viscosity agitation. However, the agitation Reynolds number was 25,000 at 600 rpm. This was due to the fact that the impeller power number of the three propeller blades was 1, which was smaller than that of other agitation blades [39]. Therefore, even if the agitation intensity was a general value, the agitation Reynolds number became larger, and energy consumption also became larger. It will be possible to optimize the rotations and electric power consumption by selecting a more suitable agitator at the similar experimental apparatus. The thermal energy storage density in the ultrasonic vibration system was not as large as that in the agitation system. The reason for this result is that it was difficult to resonate the ultrasonic transducer. To resonate the ultrasonic transducer, it is necessary to provide a natural frequency, but this frequency varies slightly depending on the environment in which the ultrasonic transducer is placed, for example, the materials in contact. Also, the natural frequency is also expected to change during the transformation of the aqueous solution into hydrate. Therefore, it is possible that the ultrasonic transducer was not able to resonate properly in this experimental system. A possible solution to solve this problem is to use a device that automatically follows the resonant frequency and keeps giving the resonant frequency to the transducer. Since the power consumption for ultrasonic vibration is about one-tenth of the power used for agitation, it is thought that the ultrasonic vibration system could be the most favorable way by solving the above problems.

3.6. The Evaluation of the Heat Exchanger

The thermal energy storage rate by the heat exchanger can be calculated as in Equation (3), where U is the heat transfer coefficient, A is the surface area of the heat exchange coil, and V_{PCM} is the volume of the thermal energy storage medium. The logarithmic mean temperature difference, ΔT_{lm}, is calculated by Equation (4). As can be seen from Equation (4), the logarithmic mean temperature difference, ΔT_{lm}, is the average of the temperature difference between the thermal energy storage medium and the cooling water using the logarithm. This logarithmic mean temperature difference was substituted into Equation (3) to calculate the heat transfer coefficient for the experiments under each condition. The heat transfer coefficient was calculated to be about 10^4–10^5 W m^{-2} K. The A/V_{PCM} in this experiment was 15 m^2/m^3, and the UA/V_{PCM} value was calculated to be around 10^3–10^4 W m^{-3} K. For instance, a plate heat exchanger has a UA/V_{PCM} that is similar to this value [40]. As the UA/V increases, the amount of heat exchange will also increase.

It realizes a higher thermal energy storage density. In this study, the UA/V of the heat exchanger was comparable to that of other common heat exchangers [40]. This result demonstrates that the comparable thermal energy storage density in this study can be obtained using other common heat exchangers.

For the practical use of thermal energy storage using TBAAc hydrate on a larger scale, it is also expected that the comparable thermal energy storage density in this study would be available by using a heat exchanger which has the same level UA/V.

$$\dot{q} = UA\Delta T_{\mathrm{lm}}/\mathrm{V}_{PCM} \tag{3}$$

$$\Delta T_{\mathrm{lm}} \frac{T_{out} - T_{in}}{ln\frac{T_{PCM}-T_{in}}{T_{PCM}-T_{out}}} \tag{4}$$

4. Conclusions

Kinetic characteristics of thermal energy storage using tetrabutylammonium acrylate (TBAAc) hydrate were practically and experimentally evaluated for practical use as Phase Change Materials (PCMs). During the experiments, the adhesion of hydrate on the surface of the heat exchanger coil was found, which increased the thermal resistance between the heat exchanger and thermal energy storage medium. This was why, as the external forces, we added a mechanical agitation (rotation rate of 100 rpm, 300 rpm, and 600 rpm) and ultrasonic vibration (frequency of 28 kHz and 56 kHz) on each system. It was revealed that the external forces improved the thermal energy storage kinetic characteristics. When the agitation rate was 600 rpm, the system achieved thermal energy storage of 140 MJ/m^3 in 2.9 h. This value is comparable to the ideal performance of ice thermal energy storage when its solid phase fraction is 45%. The energy consumption for agitation was 28 MJ/m^3 to achieve this value. The thermal energy storage of 100 MJ/m^3, which is a TBAAc solid phase fraction of 50%, was achieved in 1.5 h and 5.8 h with mechanical agitation (600 rpm) and ultrasonic vibration (28 kHz), respectively. The energy consumptions to achieve this target value were 15 MJ/m^3 and 5.2 MJ/m^3, respectively. In summary, the agitation increased the rate of heat and mass transfer by creating forced convection, thereby shortening the hydrate formation time and increasing the growth rate of the hydrate. In addition, ultrasonic vibration could keep the hydrate growth time longer by the effect of cavitation.

In this system, the UA/V (U: thermal transfer coefficient, A: surface area of the heat exchange coil, V: volume of the thermal energy storage medium) was approximately 1.0×10^{-4}–10^{-3} W m^{-3} K. This UA/V of the heat exchanger was comparable to that of other common heat exchangers. Even if the system would be scaled up and different from this study, the same level of thermal energy storage as this study could be obtained by using a heat exchanger of which UA/V is comparable to this study. As for the ultrasonic vibration system, thermal energy storage density was one-tenth of the agitated system. A device that enables an oscillator to resonate and break the hydrate adhesion is necessary to increase the thermal energy storage density. Then, that system would be most favorable in terms of the storing performance and energy power consumption.

Author Contributions: Conceptualization, H.K., H.T. and R.O.; methodology, H.T., S.I., H.N. and R.O.; formal analysis, H.T., S.I., H.N. and R.O.; investigation, H.K., H.T., S.I., H.N. and R.O.; resources, H.T. and R.O.; data curation, H.K., H.T., S.I., H.N. and R.O.; writing—original draft preparation, H.K. and R.O.; writing—review and editing, H.K. and R.O.; visualization, H.T. and R.O.; supervision, R.O.; project administration, R.O.; funding acquisition, R.O. All authors have read and agreed to the published version of the manuscript.

Funding: This work has been supported by a Keirin-racing-based research promotion fund from the JKA Foundation (Grant Number: 2020M-195) and a part of Low Carbon Technology Research and Development Program for "Practical Study on Energy Management to Reduce CO_2 emissions from University Campuses" from the Ministry of the Environment, Japan.

Institutional Review Board Statement: Not applicable.

Informed Consent Statement: Not applicable.

Data Availability Statement: Not applicable.

Acknowledgments: The authors would like to thank Haruki Sato, professor emeritus and Masao Takeuchi, Keio University, for the encouragement on this work.

Conflicts of Interest: The authors declare no conflict of interest.

References

1. IEA. *World Energy Outlook*; International Energy Agency (IEA): Paris, France, 2019.
2. Fei, F.; Qi, Q.; Liu, A.; Kusiak, A.A. Data-driven smart manufacturing. *J. Manuf. Syst.* **2018**, *48*, 157–169.
3. Król, A. The Application of the Artificial Intelligence Methods for Planning of the Development of the Transportation Network. *Transp. Res. Procedia* **2016**, *14*, 4532–4541. [CrossRef]
4. Masanet, E.; Shehabi, A.; Lei, N.; Smith, S.; Koomey, J. Recalibrating global data center energy-use estimates. *Science* **2020**, *367*, 984–986. [CrossRef] [PubMed]
5. Zimmermann, S.; Meijer, I.; Tiwari, M.K.; Paredes, S.; Michel, B.; Poulikakos, D. Aquasar: A hot water cooled data center with direct energy reuse. *Energy* **2012**, *43*, 237–245. [CrossRef]
6. Beghi, A.; Cecchinato, L.; Mana, G.D.; Lionello, M.; Rampazzo, M.; Sisti, E. Modelling and control of a free cooling system for Data Centers. *Energy Procedia* **2017**, *140*, 447–457. [CrossRef]
7. Ko, J.-S.; Huh, J.-H.; Kim, J.-C. Improvement of Energy Efficiency and Control Performance of Cooling System Fan Applied to Industry 4.0 Data Center. *Electronics* **2019**, *8*, 582. [CrossRef]
8. Khalaj, A.H.; Halgamuge, S.K. A Review on efficient thermal management of air- and liquid-cooled data centers: From chip to the cooling system. *Appl. Energy* **2017**, *205*, 1165–1188. [CrossRef]
9. Stephan, K.; Laesecke, A. The thermal conductivity of fluid air. *J. Phys. Chem. Ref. Data* **1985**, *14*, 227–234. [CrossRef]
10. Pielichowska, K.; Pielichowski, K. Phase change materials for thermal energy storage. *Prog. Mater. Sci.* **2014**, *65*, 67–123. [CrossRef]
11. Veerakumar, C.; Sreekumar, A. Phase change material based cold thermal energy storage: Materials, techniques and applications—A review. *Int. J. Refrig.* **2015**, *67*, 271–289. [CrossRef]
12. Xie, N.; Huang, Z.; Luo, Z.; Gao, X.; Fang, Y.; Zhang, Z. Inorganic Salt Hydrate for Thermal Energy Storage. *Appl. Sci.* **2017**, *7*, 1317. [CrossRef]
13. Porteiro, J.; Míguez, J.L.; Crespo, B.; Lara, J.; Pousada, J.M. On the Behavior of Different PCMs in a Hot Water Storage Tank against Thermal Demands. *Materials* **2016**, *9*, 213. [CrossRef] [PubMed]
14. Ndukwu, M.C.; Bennamoun, L.; Simo-Tagne, M. Reviewing the Exergy Analysis of Solar Thermal Systems Integrated with Phase Change Materials. *Energies* **2021**, *14*, 724. [CrossRef]
15. Wong-Pinto, L.-S.; Milan, Y.; Ushak, S. Progress on use of nanoparticles in salt hydrates as phase change materials. *Renew. Sustain. Energy Rev.* **2020**, *122*, 109727. [CrossRef]
16. Mitran, R.-A.; Ionita, S.; Lincu, D.; Berger, D.; Matei, C. A Review of Composite Phase Change Materials Based on Porous Silica Nanomaterials for Latent Heat Storage Applications. *Molecules* **2021**, *26*, 241. [CrossRef]
17. Zalba, B.; Marín, J.; Cabeza, L.; Mehling, H. Review on thermal energy storage with phase change: Materials, heat transfer analysis and applications. *Appl. Therm. Eng.* **2003**, *23*, 251–283. [CrossRef]
18. ASHRAE Technical Committee. *ASHRAE TC9.9 Data Center Power Equipment Thermal Guidelines and Best Practices*; ASHRAE: Peachtree Corners, GA, USA, 2016.
19. Arai, Y.; Yamauchi, Y.; Tokutomi, H.; Endo, F.; Hotta, A.; Alavi, S.; Ohmura, R. Thermophysical property measurements of tetrabutylphosphonium acetate (TBPAce) ionic semiclathrate hydrate as thermal energy storage medium for general air conditioning systems. *Int. J. Refrig.* **2018**, *88*, 102–107. [CrossRef]
20. Koyama, R.; Hotta, A.; Ohmura, R. Equilibrium temperature and dissociation heat of tetrabutylphosphonium acrylate (TBPAc) ionic semi-clathrate hydrate as a medium for the hydrate-based thermal energy storage system. *J. Chem. Thermodyn.* **2020**, *144*, 106088. [CrossRef]
21. Miyamoto, T.; Koyama, R.; Kurokawa, N.; Hotta, A.; Alavi, S.; Ohmura, R. Thermophysical property measurements of tetrabutylphosphonium oxalate (TBPOx) ionic semiclathrate hydrates as a media for the thermal energy storage system. *Front. Chem.* **2020**, *8*, 547. [CrossRef]
22. Koyama, R.; Arai, Y.; Yamauchi, Y.; Takeya, S.; Endo, F.; Hotta, A.; Ohmura, R. Thermophysical Properties of Trimethylolethane (TME) Hydrate as Phase Change Material for Cooling Lithium-ion Battery in Electric Vehicle. *J. Power Sources* **2019**, *427*, 70–76. [CrossRef]
23. Nakane, R.; Shimosato, Y.; Gima, E.; Ohmura, R.; Senaha, I.; Yasuda, K. Phase equilibrium condition measurements inn carbo dioxide hydrate forming system coexisting with seawater. *J. Chem. Thermodyn.* **2021**, *152*, 106276. [CrossRef]
24. Alavi, S.; Ohmura, R. Understanding decomposition and encapsulation energies of structure I and II clathrate hydrates. *J. Chem. Phys.* **2016**, *145*, 154708. [CrossRef] [PubMed]
25. Horii, S.; Ohmura, R. Continuous separation pf CO_2 from a H_2 + CO_2 gas mixture using clathrate hydrate. *Appl. Energy* **2018**, *225*, 78–84. [CrossRef]

26. Kiyokawa, H.; Horii, S.; Alavi, S.; Ohmura, R. Improvement of continuous hydrate-based CO_2 separation by forming structure II hydrate in the system of H_2 + CO_2 + H_2O + Tetrahydropyran (THP). *Fuel* **2020**, *278*, 118330. [CrossRef]
27. Hatsugai, T.; Nakayama, R.; Tomura, S.; Akiyoshi, R.; Nishitsuka, S.; Nakamura, R.; Takeya, S.; Ohmura, R. Development and Continuous Operation of a Bench-Scale System for the Production of O_3 + O_2 + CO_2 Hydrates. *Chem. Eng. Technol.* **2020**, *43*, 2307–2314. [CrossRef]
28. Nagashima, H.D.; Alavi, S.; Ohmura, R. Preservation of carbon dioxide clathrate hydrate in the presence of fructose or glucose and absence of sugars under freezer conditions. *J. Ind. Eng. Chem.* **2017**, *54*, 332–340. [CrossRef]
29. Kondo, Y.; Alavi, S.; Takeya, S.; Ohmura, R. Characterization of the Clathrate Hydrate Formed with Fluoromethane and Pinacolone: The Thermodynamic Stability and Volumetric Behavior of the Structure H Binary Hydrate. *J. Phys. Chem. B* **2021**, *125*, 328–337. [CrossRef]
30. Yamauchi, Y.; Yamasaki, T.; Endo, F.; Hotta, A.; Ohmura, R. Thermodynamic Properties of Ionic Semiclathrate Hydrate Formed with Tetrabutylammonium Propionate. *Chem. Eng. Technol.* **2017**, *40*, 1810–1816. [CrossRef]
31. Yamauchi, Y.; Arai, Y.; Yamasaki, T.; Endo, F.; Hotta, A.; Ohmura, R. Phase equilibrium temperature and dissociation heat of ionic semiclathrate hydrate formed with tetrabutylammonium butyrate. *Fluid Phase Equilib.* **2017**, *441*, 54–58. [CrossRef]
32. Sato, K.; Tokutomi, H.; Ohmura, R. Phase equilibrium of ionic semi-clathrate hydrates formed with tetrabutylammonium bromide and tetrabutylammonium chloride. *Fluid Phase Equilib.* **2013**, *337*, 115–118. [CrossRef]
33. Oyama, H.; Shimada, W.; Ebinuma, T.; Kamata, Y.; Takeya, S.; Uchida, T.; Nagao, J.; Narita, H. Phase diagram, latent heat, and specific heat of TBAB semi-clathrate hydrate crystals. *Fluid Phase Equilib.* **2005**, *234*, 131–135. [CrossRef]
34. Fujiura, K.; Nakamoto, Y.; Taguchi, Y.; Ohmura, R.; Nagasaka, Y. Thermal conductivity measurements of semi-clathrate hydrates and aqueous solutions of tetrabutylammonium bromide (TBAB) and tetrabutylammonium chloride (TBAC) by the transient hot-wire using parylene-coated probe. *Fluid Phase Equilib.* **2016**, *413*, 129–136. [CrossRef]
35. Sakamoto, H.; Sato, K.; Shiraiwa, K.; Takeya, S.; Nakajima, M.; Ohmura, R. Synthesis, Characterization and thermal-property measurements of ionic semi-clathrate hydrates formed with tetrabutylphosphonium chloride and tetrabutylammonium acrylate. *RSC Adv.* **2011**, *1*, 315–322. [CrossRef]
36. Lemmon, E.W.; McLinden, M.O. Huber M.L. NIST Reference Fluid Thermodynamic and Transport Properties (REFPROP). *J. Res. Natl. Inst. Stand. Technol.* **2013**.
37. Nakajima, M.; Hirata, A. *High-Efficient Thermal Energy Storage Technique with a Clathrate Hydrate; IHI Technical Report*; IHI: Tokyo, Japan, 2009; Volume 49, pp. 210–218.
38. Iida, Y. Sono Process no Hanashi—Chemical Engineering Applications of Ultrasonic (SCIENCE AND TECHNOLOGY). *Nikkan Kogyo Shimbun* **2006**, *7*, 7–17.
39. Hashimoto, K. *Industrial Reaction Equipment: Selection, Design, and Examples*; Baihukan: Tokyo, Japan, 1984; ISBN 9784563041618.
40. The Japan Society of Mechanical Engineers. *JSME Data Book: Heat Transfer Materials*; The Japan Society of Mechanical Engineers: Tokyo, Japan, 1986; ISBN 9784888981842.